Heterotrinuclear Oxo-Bridged $Fe^{III}ORu^{IV}OFe^{III}$ Complexes of Ruthenium Porphyrin and Borylated Low-Spin Iron Dioximes[1]

Isak Vernik and Dennis V. Stynes*

Department of Chemistry York University, North York, Ontario, Canada M3J 1P3

Received August 13, 1997[⊗]

The synthesis, structure, spectra, and reactivity of diamagnetic linear chain heterotrinuclear oxo-bridged complexes $L-Fe^{III}\ N_4-O-Ru^{IV}(TPP')-O-Fe^{III}N_4-L$ are described where TPP′ is tetrakis(4-methoxyphenylporphyrinate), N_4 is one of the borylated bis(dioximate) macrocycles, $N_4 = ((DMG)BF_2)_2$ in **1**, $((DMG)BPh_2)_2$ in **2**, and $((DPG)BF_2)_2$ in **3**, and L is a monodentate terminal ligand, L = $BuNH_2$, CH_3CN, Py, 1-MeIm, $(BuO)_3P$, etc. Crystal data for **3**-$(BuNH_2)_2$ = $[(BuNH_2)Fe((DPG)BF_2)_2-O]_2Ru(TPP')$ monoclinic space group $P2_1/n$, a = 16.845 Å, b = 27.184 Å, c = 24.593 Å, β = 90.41°, Fe−O = 1.79(1) Å, Ru−O = 1.80(1) Å, Fe−O−Ru = 175°. Large porphyrin and phenyl ring current shifts permit ready characterization of the materials by ^{1}H NMR. A red-shifted Soret band at 433 nm and two charge transfer transitions in the 650−850 nm region are observed in the visible spectra. Clean reduction of **1**, **2**, and **3**-$(CH_3CN)_2$ with 4-*tert*-butylcatechol is observed giving Fe(II) and Ru(II) products. The kinetics of reduction parallel those of low-spin (μ-oxo)diiron FeN_4 systems showing a $1/[CH_3CN]$ dependence, but the rates are 10^3-10^5 times slower. The Ru^{IV} is proposed to stabilize the μ-oxo−Fe bonds toward reductive cleavage via delocalization of the oxo π electrons onto the ruthenium. Electrochemical data for the heterotrinuclear Fe−O−Ru−O−Fe systems are compared with those for the binuclear Fe−O−Fe systems. The HOMO is stabilized by 120 mV over the corresponding Fe−O−Fe system.

Introduction

Oxo-bridged complexes play an important role in transition metal chemistry and are the functional component of many metalloproteins.[2] Binuclear Fe−O−Fe complexes are especially common in biological systems, and a variety of model systems have been described.[3] Trinuclear oxo-bridged complexes are relatively rare.[4] The best known examples are the ruthenium reds.[5] These are very stable diamagnetic $Ru^{III}-O-Ru^{IV}-O-Ru^{III}$ systems such as $[(NH_3)_5Ru^{III}ORu^{IV}(NH_3)_4ORu^{III}(NH_3)_5]^{6+}$, $[(NH_3)_5Ru^{III}ORu^{IV}(en)_2ORu^{III}(NH_3)_5]^{6+}$, and $[(bpy)_2(H_2O)Ru^{III}ORu^{IV}(bpy)_2ORu^{III}(OH_2)(bpy)_2]^{6+}$. Murray et al.[6] recently reported the synthesis and solid state magnetic properties of some new heterotrinuclear complexes formed via the oxidation of Fe^{II}(porphyrin) or Fe^{II} (Schiff base) systems with dioxoruthenium(VI) porphyrins. These materials were found to be paramagnetic and rather unstable in solution.

We previously described a new class of (μ-oxo)diiron systems[7] based upon the borylated dioxime macrocycles, Fe-$((DMG)BF_2)_2$ and $Fe((DMG)BPh_2)_2$. These μ-oxo systems, abbreviated generically as $[LFeN_4\ ]_2O$, differ from most other (μ-oxo)diiron complexes in that they are low spin, they are relatively strong oxidants, and they bind a sixth ligand (L) trans to the oxo group. We anticipated that these properties might persist in heterotrinuclear derivatives, and this is indeed the case. Here we describe the synthesis, characterization, crystal structure, and reactivity of a variety of heterotrinuclear $LFe^{III}N_4-O-Ru^{IV}-O-Fe^{III}N_4(L)$ complexes formed in the reaction of $RuTPP'(O)_2$[8] with $Fe^{II}N_4(CH_3CN)_2$.[9]

Experimental Section

Materials. Common ligands were obtained from standard sources and were used as received. Solvents were dried over molecular sieves

[⊗] Abstract published in *Advance ACS Abstracts,* December 15, 1997.

(1) Abbreviations: $(DMG)BPh_2$, (diphenylboryl)dimethylglyoximate; $(DMG)BF_2$, (difluoroboryl)dimethylglyoximate; $(DPG)BF_2$, (difluoroboryl)-diphenylglyoximate; FeN_4, a bis(glyoximato)iron complex; TPP′, 5,10,15,20-tetrakis(4-methoxyphenyl)porphyrinate; TPP, tetraphenylporphyrinate; salmah, *N*,*N*′-(4-methyl-4-azaheptane-1,7-diyl)bis-(salicylaldiminaate).

(2) (a) Holm, R. H. *Chem. Rev.* **1987**, *87*, 1401. (b) Holm, R. H.; Kennepohl, P.; Solomon, E. I. *Chem. Rev.* **1996**, *96*, 2239. (c) Yachandra, V. K.; Sauer, K.; Klein, M. P. *Chem. Rev.* **1996**, *96*, 2927.

(3) (a) Murray, K. S. *Coord. Chem. Rev.* **1974**, 12, 1−35. (b) Kurtz, D. M.*Chem. Rev.* **1990**, *90*, 585−606. (c) Vincent, J. B.; Olivier-Lilley, G. L.; Averill, B. A. *Chem. Rev.* **1990**, *90*, 1447−1467. (d) Waller, B. J.; Lipscomb, J. D. *Chem. Rev.* **1996**, *96*, 2625.

(4) (a) Fenton, D. E.; Okawa, H. *J. Chem. Soc., Dalton Trans.* **1993**, 1349. (b) Trautwein, A. X.; Bill, E.; Bominaar, E. L.; Winkler, H. *Struct. Bonding* **1991**, *78*, 1. (c) Messerschmidt, A. *Adv. Inorg. Chem.* **1994**, *40*, 121. (d) Coleman, J. E.; Gettins, P. In *Metals in Biology*; Spiro, T. G., Ed.; Wiley: New York, 1983; Vol. 3, Chapter 5. (e) Bill, E.; Krebs, C.; Winter, M.; Gerdan, M.; Trautwein, A. X.; Florke, U.; Haupt, H.; Chaudhuri, P. *Chem. Eur. J.* **1997**, *3*, 193.

(5) (a) Fletcher, J. M.; Greenfield, F.; Hardy, C. J.; Scargill, D.; Woodhead, J. L.; *J. Chem. Soc.* **1960**, 2000. (b) Smith, P. M.; Fealey, T.; Earley, J. E.; Silverton, J. V. *Inorg. Chem.* **1971**, *10*, 1943. (c) Earley, J. E.; Fealey, T. *Inorg. Chem.* **1973**, *12*, 323. (d) Geselowitz, D. A.; Kutner, W.; Meyer, T. J. *Inorg. Chem.* **1986**, *25*, 2015.

(6) (a) Berry, K. J.; Moubaraki, B.; Murray, K. S.; Nichols P. J.; Schulz, L. D.; West, B. O. *Inorg. Chem.* **1995**, *34*, 4123. (b) Schulz, L. D.; Fallon, G. D.; Moubaraki, B.; Murray, K. S.; West, B. O. *J. Chem. Soc., Chem. Commun.* **1992**, 971.

(7) (a) Stynes, D. V.; Noglik, H.; Thompson, D. W. *Inorg. Chem.* **1991**, *30*, 4567. (b) Noglik, H.; Thompson, D. W.; Stynes, D. V. *Inorg. Chem.* **1991**, *30*, 4571. (c) Vernik, I.; Stynes, D. V. *Inorg. Chem.* **1996**, *35*, 2006. (d). Vernik, I.; Stynes, D. V. *Inorg. Chem* **1996**, *35*, 2011. (e) Vernik, I.; Stynes, D. V. *Inorg. Chem.* **1996**, *35*, 1093. (f) Vernik, I.; Stynes, D. V. *Inorg. Chem* **1996**, *35*, 6210.

(8) (a) Groves, J. T.; Quinn, R. *Inorg. Chem.* **1984**, *23*, 3844. (b) Leung, W.; Che, C. *J. Am. Chem. Soc.* **1989**, *111*, 8812. (c) Ho, W.; Leung, W.; Che, C. *J. Chem. Soc., Dalton Trans.* **1991**, 2933.

(9) (a) Thompson, D. W.; Stynes, D. V. *Inorg. Chem.* **1990**, *29*, 3815. (b) Stynes, D. V. *Inorg. Chem.* **1994**, *33*, 5022. (c) de Silva, D. G. A. H.; Leznoff, D. B.; Impey, G. A.; Vernik, I.; Jin, Z.; Stynes, D. V. *Inorg. Chem.* **1995**, *34*, 4015. (d) Segal, G.; Stynes, D. V. Unpublished results

S0020-1669(97)01016-1 CCC: $15.00
Published on Web 01/12/1998

(3 Å). Tetrakis(4-methoxyphenyl)porphyrin (H_2TPP') was prepared by standard methods,[10] and ruthenium insertion was carried out using the $RuCl_3$ method[11] to give $Ru(TPP')(CO)(C_2H_5OH)$. The iron complexes $Fe^{II}((DMG)BR_2)_2(CH_3CN)_2$ (R= F, Ph) were prepared as described previously.[9] $Fe((DPG)BF_2)_2(CH_3CN)_2$ was a gift of Gersana Segal.[9d]

Physical Measurements. Visible spectra were recorded on an Aminco DW-2a UV−vis, Cary 2400, or Hewlett Packard 8452A spectrophotometer in 1 cm Pyrex or quartz cuvettes thermostated at 25 °C. The ^1H NMR spectra were obtained on a Bruker ARX 400 MHz spectrometer at 300 K using $CDCl_3$ as the solvent with TMS as an internal standard.

Electrochemistry. Electrochemical data were collected with a Princeton Applied Research Corp. model 263 potentiostat/galvanostat. Cyclic voltammetry experiments were performed under a nitrogen atmosphere in CH_2Cl_2 solution containing 0.1 M $(TBA)PF_6$ and ~5×10^{-3} M complex. A platinum disk sealed in glass was used as a working electrode. Platinum wire was used as a counter electrode, and AgCl/Ag was used as the quasi-reference electrode. Ferrocene was used as an internal reference ($Fc^+/Fc = 0.46$ V in CH_2Cl_2 vs SCE[12]).

$[Ru^{VI}(O)_2(TPP')]$ was prepared by the method of Che.[8b] $Ru(TPP')(CO)(EtOH)$ (60 mg, 0.066 mmol) was dissolved in a CH_2Cl_2/EtOH mixture (9:1, 20 mL). The solution was added to a solution of *m*-chloroperoxobenzoic acid (3 g) in EtOH (100 mL). After 1 h, a purple precipitate was filtered out and washed several times with EtOH. Yield: 35 mg, 61%. The product was found to be sensitive to the trace amounts of acid commonly present in $CDCl_3$, and when stored at room temperature in air, it slowly converted to $HORu^{IV}ORu^{IV}OH$ within days, but when stored at −20 °C in vacuo, it was stable for months. ^1H NMR ($CDCl_3$, δ (ppm)): H_β 9.10 (s), H_o 8.25 (d), H_m 7.35 (d), OCH_3 4.13 (s). Vis (CH_2Cl_2, λ (nm)): Soret 426, α 525, β 556.

1-$(CH_3CN)_2$. $Ru(O)_2TPP'$ (55 mg, 6.3×10^{-2} mmol) was dissolved in N_2-purged CH_2Cl_2 (15−20 mL), and $Fe((DMG)BF_2)_2(CH_3CN)_2$ (58 mg, 0.125 mmol) was added to the purple solution. The solution slowly turned a blue-green, and after 30 min, unreacted $Fe((DMG)BF_2)_2(CH_3CN)_2$ was filtered off and acetonitrile (~1 mL) was added to the filtrate. Hexane (75 mL) was then slowly added, depositing a dark green precipitate. This was filtered out and dried in vacuo. Yield: 94 mg, 87%.

4-$(CH_3CN)_2$ was prepared as above. In a typical preparation, $Ru(O)_2TPP'$ (105 mg, 0.121 mmol) and $Fe((DMG)BPh_2)_2(CH_3CN)_2$ (160 mg, 0.230 mmol) were reacted. Yield: 200 mg, 80%.

5-$(CH_3CN)_2$. was prepared as above. In a typical preparation, $Ru(O)_2TPP'$ (89 mg, 0.103 mmol) and $Fe((DPG)BF_2)_2(CH_3CN)_2$ (150 mg, 0.205 mmol) reacted.Yield: 156 mg, 67%.

Various ligated derivatives of **1**, **2**, or **3** were generated in situ by addition of excess ligand to the CH_3CN-ligated derivative in dichloromethane solution. Visible and NMR spectral data for all derivatives are collected in Tables 1 and 2. Solid samples were obtained by precipitation with hexane. All complexes tended to retain solvent, so the visible and NMR spectra provided better criteria of purity than elemental analyses.

Crystallography. Numerous attempts were made to grow crystals of the various derivatives of **1** and **2** without success. The diphenylglyoxime system was selected to provide a molecular shape perhaps more suited to crystal packing. Crystals of **3**-$(BuNH_2)_2$ were finally obtained by slow diffusion of hexanes into a CH_2Cl_2 solution of the complex. Crystals rapidly lost solvent unless coated immediately with epoxy cement and were weakly diffracting. Intensity data were collected locally on a Siemens R3m/v diffractometer using graphite-monchromatized Mo Kα radiation and also on a SMART CCD system at the Windsor facility.[13a] Both data sets refined similarly, but only results for the larger CCD set are reported here. Structure solution and refinement used the SHELXTL Plus and SHELX93 software[13] with final anisotropic refinement on F^2. Hydrogen atoms were included in calculated positions using a riding model with C−H distances of 0.96 Å and fixed isotropic thermal parameters of 0.08 $Å^2$. Several difference peaks of ~1 e/$Å^3$ were located in channels running between the trinuclear molecules. These appeared to be disordered hexane solvent molecules (confirmed by NMR), but no satisfactory model could be found. The presence of diffuse solvent necessarily produces a poor fit of the low-angle data.[14] Several approaches were examined, but none gave a dramatic improvement in *R*. The relevant structural features of **3**-$(BuNH_2)_2$ were insensitive to these, and therefore we ultimately selected a refinement which excluded solvent atoms and omitted low-angle data. Details are given in Table 3 and in the Supporting Information.

Table 1. Visible Spectral Data (λ_{max}, nm)

compd	Soret	α, β	CT1	CT2	Fe−O−Fe[c]
1-$(H_2O)_2$	434	538, 576	670	790	
1-$(CH_3CN)_2$[a]	435	541, 578	691	812	672
1-$(Py)_2$	435	543, 579	716		708
1-$(1\text{-MeIm})_2$	435	541, 576	703	857	688
1-$(BuNH_2)_2$	435	539, 575	694	839	689
1-$((BuO)_3P)_2$	435	546, 580	720		
2-$(H_2O)_2$	433	538, 572	698	810	672
2-$(CH_3CN)_2$	433	538, 576	709	839	687
2-$(Py)_2$	432	537, 572	719	863	728
2-$(1\text{-MeIm})_2$	435	538, 572	732	890	703
2-$(BuNH_2)_2$	435	538, 570	729	868	706
2-$(NH_3)_2$	434	537, 572	716	850	695
3-$(CH_3CN)_2$	433	544, 577	686	799	682
3-$(1\text{-MeIm})_2$	433	542, 577	714	836	704
3-$(BuNH_2)_2$	433	542, 578	710	824	704
3-$((BuO)_3P)_2$	433	541, 579	717	894	
$[Fe(salmah)O]_2Ru(TPP)$[b]	416	531, 570			

[a] Extinction coefficients for **1**-$(CH_3CN)_2$ ($\log(\epsilon)$): 5.14, 4.27, 4.23, 4.42, and 4.20 for Soret, α, β, CT1, and CT2, respectively. Other derivatives of **1** and **2** give comparable values. [b] Reference 6a. [c] Reference 7d.

Kinetic Measurements. A dichloromethane solution of 4-*tert*-butylcatechol was injected via syringe into a thermostated (25 °C) CH_3CN solution of **1**, **2**, or **3** (1×10^{-5} M), and the subsequent reaction was followed by visible spectroscopy. Spectra were typically scanned between 350 and 800 nm (displaying clean isosbestic points), or they were monitored at wavelengths of maximum absorbance change. Pseudo-first-order rate constants were obtained typically using the decay at 700 nm by means of a least-squares analysis. Kinetic results were found to be generally unaffected by oxygen, and most experiments were carried out in air.

Results and Discussion

Synthesis. The synthetic route to these heterotrinuclear oxo-bridged complexes relies on the facile inner-sphere oxidation of labile Fe^{II} complexes by dioxo Ru^{VI} porphryins.[8] This route was previously used by Murray et al. in which high-spin heme or Fe(Schiff base) systems were linked to O−Ru−O.[6] The low-spin but labile[9a] $FeN_4(CH_3CN)_2$ precursors are sparingly soluble in CH_2Cl_2, but addition of $Ru^{VI}(O)_2(TPP')$ causes the quick dissolution of both reagents, forming the soluble trinuclear complexes **1, 2**, and **3** in their CH_3CN-ligated forms. (See eq 1 and Figure 1.) The reaction is sufficiently clean that a relatively pure product is obtained merely by mixing the reagents

(10) Adler, A. D.; Longo, F. R.; Finarelli, J. D.; Goldmacher, J.; Assour, J.; Korskakoff, L. *J. Org. Chem.* **1967**, *32*, 476.
(11) Collman, J. P.; Barnes, C. E.; Brothers, P. J.; Collins, T. J.; Ozawa,T.; Gallucci, J. C.; Ibers, J. A. *J. Am. Chem. Soc.* **1984**, *106*, 5151.
(12) Connelly, N. G.; Geiger, W. E. *Chem. Rev.* **1996**, *96*, 877.
(13) (a) Data were collected by Glenn Yap of the University of Windsor Crystallographic Centre, Windsor, Ontario, Canada, using the Siemens SMART CCD system (Siemens Analytical X-ray Instruments Inc., Madison WI). (b) Sheldrick, G. M. *SHELXTL PC*, Version 4.1; Siemens Analytical X-Ray Instruments Inc.: Madison, WI. *SHELXL 93: program for structure refinement*; University of Göttingen, Göttingen, Germany, 1993.
(14) Driessen, H.; Haneef, M. I. J.; Harris, G. W.; Howlin, B.; Khan, G.; Moss, D. S. *J. Appl. Crystallogr.* **1989**, *22*, 510.

Table 2. 400 MHz ^{1}H NMR Data (δ, ppm)[a]

compd	H_β	H_o	H_m	OCH_3	DMG CH_3	ligand	BPh_2 eq H_o	BPh_2 eq H_m	BPh_2 eq H_p	BPh_2 ax H_o	BPh_2 ax H_m	BPh_2 ax H_p
1-$(H_2O)_2$	9.13	8.66	7.47	4.17	1.487	−0.95						
1-$(CH_3CN)_2$	9.17	8.74	7.48	4.17	1.482	1.10						
1-$(CH_3CH_2CH_2CN)_2$	9.16	8.73	7.46	4.15	1.46	α 1.36, β 0.71, γ 0.096						
1-(1-MeIm)$_2$	9.20	8.77	7.46	4.15	1.56	Me 2.83, H2 4.87, H4 4.49, H5 5.72						
1-$(Py)_2$	9.29	8.78	7.48	4.16	1.67	H_o 5.55, H_m 6.19, H_p 6.89						
1-$(Py)(CH_3CN)$	*c*	*c*	*c*	4.16	1.62, 1.50	*c*						
2-$(D_2O)_2$[b]	8.51	8.77	7.42	4.20	1.80		7.49	7.49	7.30	5.90	6.19	6.19
2-$(CD_3CN)_2$	8.24	9.01	7.38	4.20	1.67		7.44	7.44	7.15	6.12	6.27	6.09
2-(1-MeIm)$_2$[b]	8.26	9.04	7.49	4.23	1.80	Me 1.98, H2 3.64, H4 3.58, H5 3.96						
2-(Py-d_5)$_2$[b]	8.58	9.12	7.59	4.16	2.09		7.48	7.43	7.35	5.73	5.92	5.96
2-$(NH_3)_2$	8.34	8.90	7.52	4.22	1.69	NH_3 −3.64	7.50	7.50	7.29	6.00	6.32	6.30
2-$(BuNH_2)_2$	8.22	8.99	7.52	4.24	1.74	NH_2 −1.85, α −1.13, β −2.59, γ −0.34, δ −0.11 (confirmed by COSY)	7.52	7.46	7.25	6.24	6.39	6.39
3-$(CD_3CN)_2$	9.11	8.02	7.10	4.13			6.44	6.81	7.10			
3-(1-MeIm)$_2$	9.13	8.11	7.07	4.11		Me 2.74, H2 5.18, H4 4.80, H5 5.73	6.54	6.87	7.15			
3-$(BuNH_2)_2$	9.12	8.01	7.08	4.11		NH_2 −0.38, α = β = γ 0.30, δ 0.18	6.54	6.88	7.17			
Ru^{VI}(TPP′)$(O)_2$	9.09	8.25	7.35	4.13								
Ru(TPP′)$(BuNH_2)$CO	8.64	8.10 7.98	7.21	4.08		NH_2 −5.79, α −3.12, β −1.60, γ −0.68, δ −0.25						
Ru^{II}(TPP′)(Py)CO	8.62	8.11 7.93	7.19	4.07		H_o 1.51, H_m 5.16, H_p 6.05						
$Fe^{II}((DMG)BF_2)_2(Py)_2$[d]					2.80	H_o 7.59, H_m 6.36, H_p 6.96						
$Fe((DMG)BPh_2)_2(Py)_2$[e]					2.79	H_o 7.74, H_m 6.98, H_p 7.47						

[a] In $CDCl_3$ at 300 K. [b] In CD_2Cl_2 at 300 K. [c] Overlapping resonances not assigned. [d] Reference 9a. [e] Reference 9c.

Table 3. Crystallographic Data for **3**-$(BuNH_2)_2$

formula	$RuFe_2C_{112}H_{98}N_{14}O_{14}B_4F_8$
fw	2272.05
space group	$P2_1/n$
a, Å	16.8450(1)
b, Å	27.1837(2)
c, Å	24.9525(1)
β, deg	90.408(1)
V, Å^3	11425.70(12)
Z	4
temp, °C	25
radiation	Mo Kα, λ(Kα$_1$) = 0.710 73 Å
linear abs coeff, mm^{-1}	0.460
transm factors	0.200−0.319
d(calcd), g/cm^3	1.321
crystal dimensions, mm	0.1 × 0.1 × 0.1
scan method	ω; 0.3° intervals over a 180° range
2θ limits	$2.84 < 2\theta < 57$
data ranges in *h*, *k*, *l*	$-20 \le h \le 21$, $-19 \le k \le 36$, $-31 \le l \le 32$
unique data, R_{int}	27233, 0.1393
resolution range	6.5−0.95
unique data	13 796
unique data ($F_o^2 > 4\sigma(F_o^2)$)	10 534
final no. of variables/restraints	1274/7
$R(F)$ ($F_o^2 > 4\sigma(F_o^2)$)	0.1208
$R_w(F)$ ($F_o^2 > 4\sigma(F_o^2)$)	0.2933
goodness of fit (F_o^2)	1.252
largest diff peak and hole, e/Å^3	1.278, −0.566

in the proper stoichiometry. The reaction involves a formal two-electron reduction of the $Ru^{VI}(O)_2$(TPP′P) to Ru^{IV} and two one-electron oxidations of Fe^{II} to Fe^{III}.

$$2FeN_4(CH_3CN)_2 + Ru(O)_2TPP' \rightarrow (CH_3CN)FeN_4{-}O{-}RuTPP'{-}O{-}FeN_4(CH_3CN) + 2CH_3CN \quad (1)$$

Electronic Spectra and Magnetism. The new complexes are all diamagnetic, in contrast to the (μ-oxo)diiron systems, $(LFeN_4)_2O$, which are paramagnetic with an $S = 1$ ground state. They are far more stable than the paramagnetic Fe−O−RuTPP−O−Fe systems of Murray,[6] which involve high-spin Fe^{III} units linked to O-Ru−O. The various ligated derivatives of **1**, **2**, and **3** are close analogues of the diamagnetic ruthenium reds, which are considered to be $Ru^{III}{-}O{-}Ru^{IV}{-}O{-}Ru^{III}$. The FeN_4 systems are known to favor a low-spin state in both oxidation states II and III, and this is also the case here.

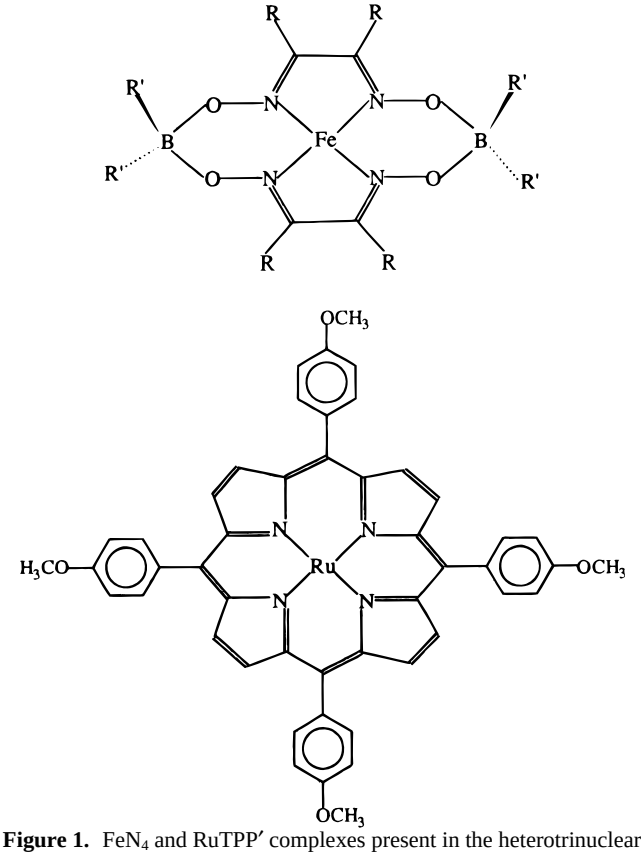

Figure 1. FeN_4 and RuTPP′ complexes present in the heterotrinuclear systems: $Fe((DMG)BF_2)_2$ in **1**, $Fe((DMG)BPh_2)_2$ in **2**, and $Fe((DPG)BF_2)_2$ in **3**.

The difference in magnetism of the binuclear $(L)FeN_4{-}O{-}FeN_4(L)$ systems and trinuclear $(L)FeN_4{-}O{-}Ru(TPP')-O-$

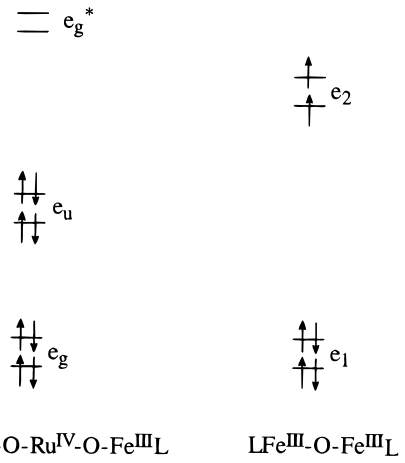

Figure 2. Simplified MO diagram for metal axial dπ orbitals in linear bi- and trinuclear complexes (adapted from Earley[5c]).

FeN_4(L) systems may be understood in terms of the simplified MO diagram adapted from Earley[5c] and given in Figure 2. Axial dπ orbitals (d_{xz} and d_{yz}) extend over the ruthenium, both iron atoms, and both oxo groups. Ignoring the pair of electrons assumed to occupy d_{xy} on each metal leaves six dπ electrons to occupy e_1 and e_2 for a linear Fe−O−Fe, leading to a triplet. In Fe−O−Ru−O−Fe there are eight dπ electrons occupying the e_g and e_u MO's, leading to a predicted singlet ground state.

The visible spectra of the trinuclear species show features characterstic of both the RuTPP′ and the $[LFeN_4]_2O$ systems. Data are collected in Table 1, and a figure is provided as supporting information. The porphyrin bands for the different ligated forms appear at similar positions, with the Soret band experiencing a significant red shift relative to those of other Ru^{IV} or Ru^{VI} porphyrins. The red-shifted Soret band for the ligated derivatives of **1**, **2**, and **3** is unusual[15] and is reminiscent of "hyper" spectra characteristic of cytochrome P-450 and bis(phosphine) derivatives of Fe^{II} or Ru^{II} porphyrins.[16] Interaction of a charge transfer state with the $a_{1u}(\pi)$, $a_{2u}(\pi) \rightarrow e(\pi)$ porphyrin transition is usually invoked to account for these red shifts.[16] Low-energy bands CT1 and CT2 at 650 −750 nm are assigned to charge transfer transitions. The shorter wavelength band resembles a corresponding feature found in (μ-oxo)diiron derivatives and is assigned to oxo to iron CT. There is a slight shift to the red of 10−20 nm compared to the band of the Fe−O−Fe analogue.

The second band, CT2, lies well into the near-IR and is not found in the spectra of the binuclear complexes. We tentatively assign this band to a transition involving the e_u and e_g* orbitals in Figure 2. Support for this assignment comes from the electrochemical data presented below. The difference in potential for the first oxidation and first reduction of ∼1.5 eV may be taken as an estimate of the HOMO/LUMO gap and can be used to estimate the position of the e_u−e_g* transition. The calculated wavelength of ∼830 nm is in good agreement with the positions of CT2 given in Table 1. The CT2 band is somewhat broader than the CT1 band, and the relative intensity of the two bands varies among **1**, **2**, and **3** but not for the different ligated derivatives within a system. Variations in the Fe−O−Ru bending in response to the different peripheral contacts in the three systems may be responsible. The positions of both CT bands are sensitive to the nature of the terminal ligands, suggesting that MO's with substantial Fe character are involved.

Table 4. Electrochemical Data for Trinuclear and Binuclear Oxo-Bridged Complexes

		Fe−O−Ru−O−Fe			Fe−O−Fe[c]	
		$E_{1/2}$,[a] V		E_p,[b] V	$E_{1/2}$,[a] V	E_p,[b] V
N_4	L					
$((DMG)BF_2)_2$	CH_3CN	0.840	1.20	−0.50	1.10	0.24
$((DMG)BPh_2)_2$	CH_3CN	0.60	1.06	−0.78	0.83	−0.30
	NH_3	0.505	1.04	−0.97	0.62	
$((DPG)BF_2)_2$	CH_3CN	1.0				

[a] Half-wave potentials for reversible oxidations. [b] Cathodic peak potential for irreversible reduction. [c] Jin, Z.; Stynes, D. Unpublished results.

Table 5. Comparison of Structural Data for μ-Oxo Fe and Ru Complexes

	3-$(BuNH_2)_2$	(RuTPP)-(O−Fe(Sal))$_2$	[(RO)-RuTPP]$_2$O[a]	[$(BuNH_2)$-$FeN_4]_2$O[b]
ref	this work	6b	11	7c
Ru−O	1.80	1.866	1.789	
Fe−O	1.788	1.848		1.766
M−O−M	175	155	177.8	178.6
ΔFe	0.06	0.16		0.026
ΔRu	0.014	0.0	0.07	
Fe−N_{ax}	2.07			2.070

[a] RO = *p*-$OC_6H_4CH_3$. [b] N_4 = $((DMG)BPh_2)_2$.

Electochemistry. Cyclic voltammetry measurements in dichloromethane show two reversible oxidation waves and an irreversible reduction wave for the CH_3CN-ligated trinuclear complexes of **1**, **2**, and **3**. The electrochemical data are summarized in Table 4. Reduction adds an electron to an antibonding orbital (see Figure 2), which normally results in irreversible oxo bridge cleavage.[7a,17] The oxidation waves are tentatively assigned to the successive $Fe^{III/IV}$ oxidations, although formal oxidation state assignments are not easily made in delocalized systems. Oxidation is expected to strengthen the μ-oxo bridge because a nonbonding or weakly antibonding electron is removed.

The electrochemical results show trends similar to those for FeN_4−O−FeN_4 systems. The potentials depend on both the N_4 and axial ligands bound to Fe. Additional studies are planned to characterize the higher oxidation level and mixed-valence species and to exploit the ability easily to alter the redox character of these trinuclear systems via changes in the ligands bound to the terminal iron atoms.

Crystallography. Crystallographic studies confirm the proposed trinuclear structure for **3**-$(BuNH_2)_2$. (See Figure 3.) Details are given in Tables 3 and 5 and in the supporting information. The trinuclear molecule lies in a general position in $P2_1/n$. The FeN_4 fragments each have a $BuNH_2$ ligand bound trans to the oxo group, and they adopt the C_{2v} conformation with axial B−F groups on the side away from the bulkier

(15) Neither diamagnetic $(HORuTPP)_2O$[11] nor paramagnetic Fe−O−RuTPP−O−Fe systems[6] show a red shift of the Soret band.

(16) (a) Ohya, T.; Morohoshi, H.; Sato, M. *Inorg. Chem.* **1984**, *23*, 1303. (b) Hanson, L. K.; Eaton, W. A.; Sligar, S. G.; Gunsalus, I. C.; Gouterman, M.; Connell, C. R. *J. Am. Chem. Soc.* **1976**, *98*, 2672. (c) Loew, G. H.; Roemer, M. *J. Am. Chem. Soc.* **1980**, *102*, 3655. (d) Antipas, A.; Buchler, J.; Gouterman, M.; Smith, P. D. *J. Am. Chem. Soc.* **1978**, *100*, 3015.

(17) Stable mixed-valent Fe^{II}−O−Fe^{III} is observed in cases involving a supported oxo bridge, but only recently has an unsupported example been reported: (a) Bossek, U.; Hummel, H.; Weyhermüller, T.; Bill, E.; Wieghardt, K. *Angew. Chem., Int. Ed. Engl.* **1995**, *34*, 2642. (b) Cohen, J. D.; Payne, S.; Hagen, K. S.; Sanders-Loehr, J. *J. Am. Chem. Soc.*, **1997**, *119*, 2960. (c) Müller, M.; Eckhard, B.; Weyhermüller, T.; Wieghardt, K. *Chem. Commun.* **1997**, 705.

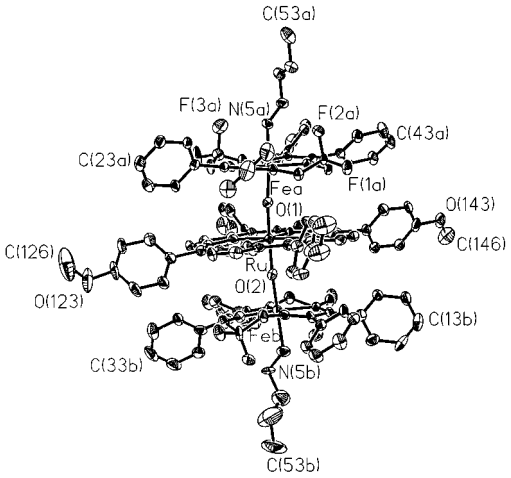

Figure 3. X-ray structure of **3**-$(BuNH_2)_2$.

O−RuTPP′ fragment. Some metrical details are compared with other μ-oxo iron and ruthenium systems in Table 5. The Ru atom is displaced slightly 0.014 Å above the porphyrin N_4 plane toward O(1). The two Ru−O bonds are essentially the same length (1.80 Å), being marginally longer than those found in a binuclear RuORu but 0.06 Å shorter than the Ru−O bonds in a RuTPP′$(OFesalmah)_2$ structure reported by West.[6b] The Ru−O−Fe bond angle shows a slightly greater deviation from linearity than found in the binuclear Fe−O−Fe and Ru−O−Ru systems given in the Table. In contrast the RuTPP′-$(OFesalmah)_2$ structure has a 155° bond angle. We do not attach a great significance to the slight bending in these systems, which likely reflects nonbonded interactions of peripheral groups.

The two iron atoms are each displaced 0.06 Å toward the oxo group. The two Fe−O bonds are essentially the same length, and they are much shorter than those found for the high-spin Fe−O−Ru−O−Fe systems of Murrray et al. The trans Fe−N bonds are normal, resembling those observed for $BuNH_2$ bound to Fe−O−Fe. The axial views in Figure 4 show that the two FeN_4 units are mutually staggered with one set of DPG phenyls and one BF_2 group lying above or below each of the four pyrrole rings. This rotamer would appear to minimize nonbonded contacts between the phenyl groups of the tetradentate macrocyclic ligands. The most significant interplanar contacts involve ortho hydrogen atoms of the phenyl rings. The displacements of atoms in the TPP′ and FeN_4 macrocycles above or below each N_4 plane are shown in Figure 5. One FeN_4 fragment (a) adopts a "domed" distortion while the other (b) might be described as "buckled". These distortions along with the slight bend in the Fe−O−Ru bonds are likely a reponse to phenyl−phenyl contacts between the $Fe((DPG)BF_2)_2$ and RuTPP′ units.

NMR Spectra. The ^{1}H NMR spectral data for a variety of ligated forms of **1**, **2**, and **3** are collected in Table 2, and a typical spectrum is shown in Figure 6 The ^{1}H NMR provides definitive characterization of the various trinuclear species and shows no indication of the peak broadening and large paramagnetic shifts characteristic of the $[LFeN_4]_2O$ complexes.[7] Integration establishes that there are two FeN_4 units for each RuTPP′ and one ligand L per Fe. A single set of TPP′ ortho and meta signals is observed. This requires a symmetrical ligation enviroment about ruthenium, as phenyl rotation is normally slow, producing split peaks in Ru(TPP′)XY derivatives.

Porphryin and phenyl (DPG and BPh_2) ring current shifts (rcs) provide a large chemical shift differentiation among the

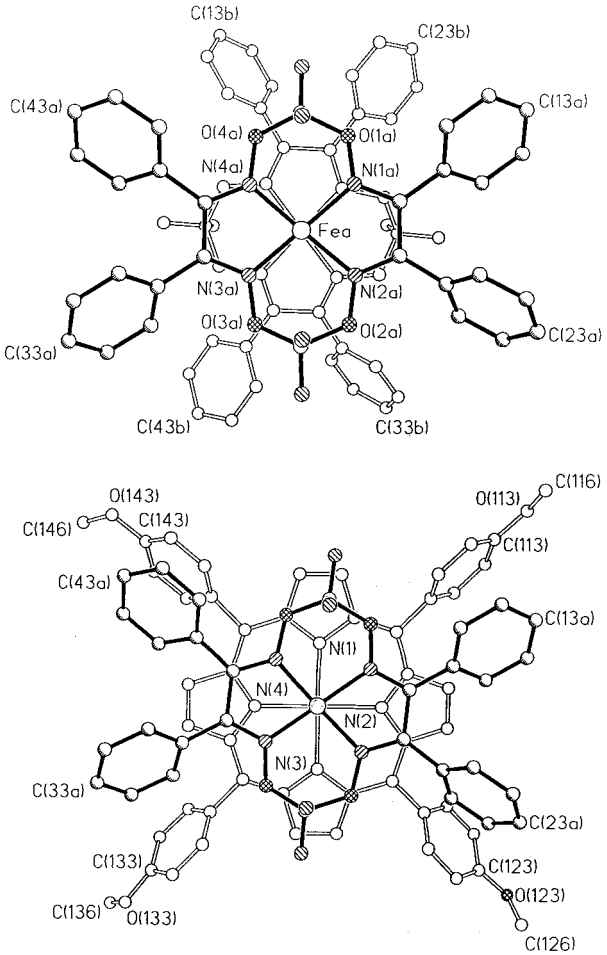

Figure 4. Axial views of **3**-$(BuNH_2)_2$ with the central RuTPP' moiety (top) and one of the terminal FeN_4 moieties (bottom) removed for clarity.

various derivatives. Observed shifts are consistent with TPP′ ring current shift calculations we have carried out on the basis of the Abraham model[18] and structural data.[7f] A semiquantitative representation of the porphyrin ring currrent effects is given in Figure 7. The DMG methyl resonances are found 1 ppm upfield of their normal position for diamagnetic FeN_4L_2 complexes (average coordinates $z = 3.8$, $\rho = 4.2$ in Figure 7). Other chemical shift effects assigned to ring current effects include the following. (a) The TPP′ H_β resonances are at 9 ppm except for derivatives of **2**. Here equatorial phenyls of BPh_2 groups lie over the H_β, producing upfield shifts of 0.5−1 ppm. (b) Ortho and meta TPP′ phenyl proton resonances lie at 8.7 and 7.5 ppm, respectively, except for derivatives of **3**, where DPG phenyls flank the TPP′ phenyls (see Figure 3), producing upfield shifts of about 1 ppm. (c) The 1-MeIm methyl resonance lies at 2.8 ppm for **1** and **3** (shifted 0.8 ppm upfield from that of the free ligand by the TPP′ ring anisotropy). For **2**-$(MeIm)_2$, the imidazole methyl resonance lies at 1.98 ppm, as the methyl is sandwiched between the axial phenyls of the BPh_2 groups. (d) Axial ligand resonances all display upfield shifts relative to those of simple $Fe^{II}N_4$ derivatives. The above features also provide a good indication of the predominant conformations in solution. For example c confirms a C_{2v}

(18) (a) Abraham, R. J.; Bedford, G. R.; McNeillie, D.; Wright B. *Org. Magn. Reson.* **1980**, *14*, 418. (b) Abraham, R. J.; Bedford, G. R.; Wright, B. *Org. Magn. Reson.* **1982**, *18*, 45. (c) Abraham, R. J.; Medforth, C. J.; Smith, K. M.; Goff, D. A.; Simpson, D. J. *J. Am. Chem. Soc.* **1987**, *109*, 4786.

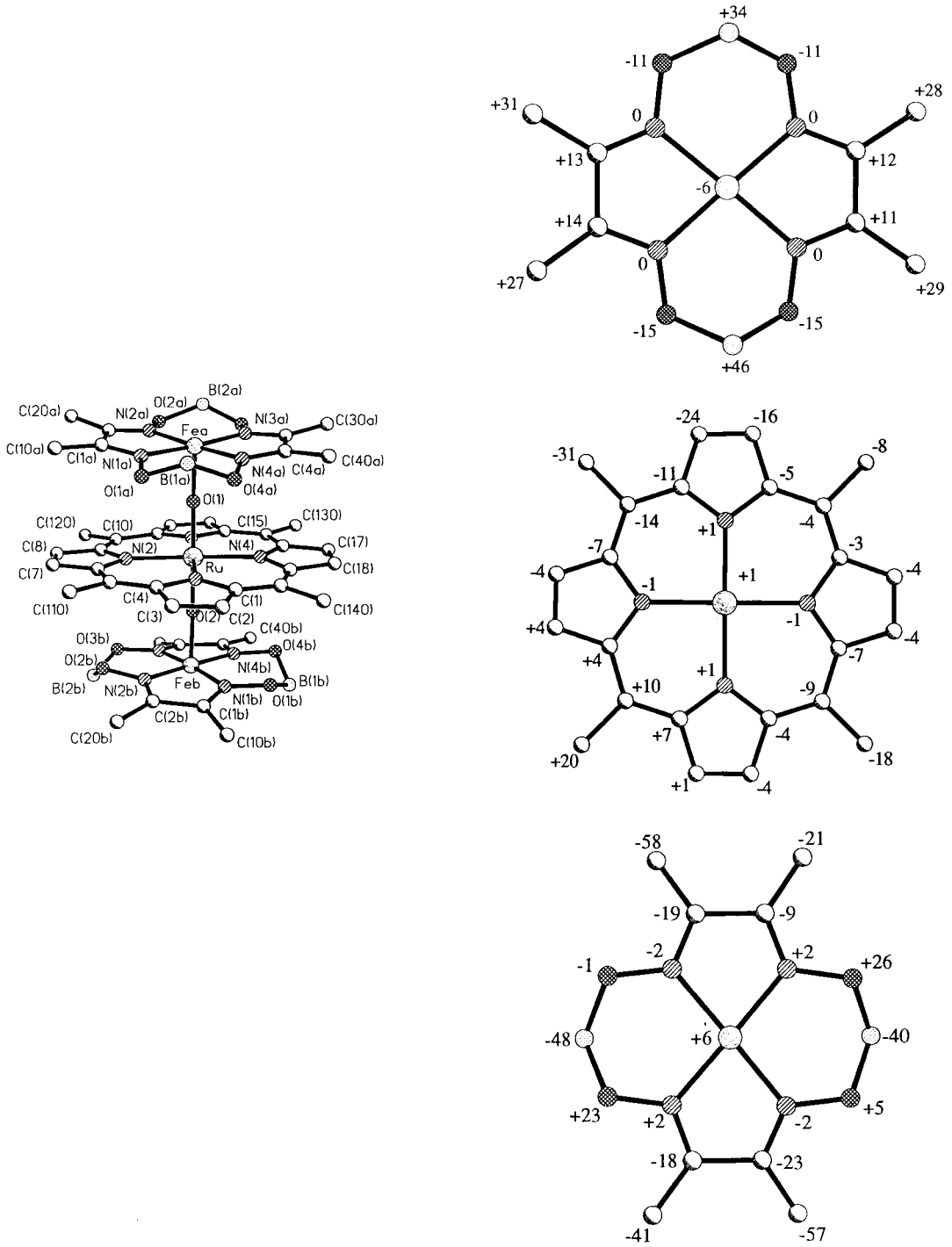

Figure 5. Perpendicular displacements in units of 0.01 Å of atoms from each of the three macrocycle N_4 planes in **3**-$(BuNH_2)_2$: top, FeN_4; middle, RuTPP′; bottom, FeN_4. Each structure is oriented as shown in the labeled trinuclear structure.

geometry and observations a and b are consistent with the dominant rotamers about the principal axis being those shown in Figure 4.

Reactions. The FeN_4-based heterotrinuclear complexes are substantially more stable in solution than paramagnetic heme- or Fe(Schiff base)-derived Fe−O−Ru−O−Fe systems yet are much better oxidants than the latter, ruthenium reds, or binuclear μ-oxo ruthenium(IV) porphyrins. The enhanced reactivity is primarily associated with the FeN_4 chemistry. Qualitative observations, such as evidence of slow exchange in the ^{1}H NMR spectra, suggest the axial ligands are bound somewhat more strongly than those in the $[LFeN_4]_2O$ systems but the axial ligands are still readily exchanged, affording a variety of ligated species. This property is especially advantageous with respect to the development of their chemistry in solution.

Kinetics of Reductive Cleavage. The binuclear μ-oxo FeN_4 derivatives were previously found to undergo clean reductive cleavage with catechols or hydroquinones, and this is also the case for the heterotrinuclear complexes. We have investigated the kinetics of reductive cleavage of the trinuclear systems by 4-*tert*-butylcatechol (H_2Q) for comparison with the corresponding reactions of the (μ-oxo)diiron derivatives. Reactions were monitored by visible spectroscopy. Typical spectral data are shown in Figure 8. The reactions proceed cleanly with isosbestic points according to eq 2. The Fe^{II} and Ru^{II} products were identified on the basis of distinctive visible and ^{1}H NMR

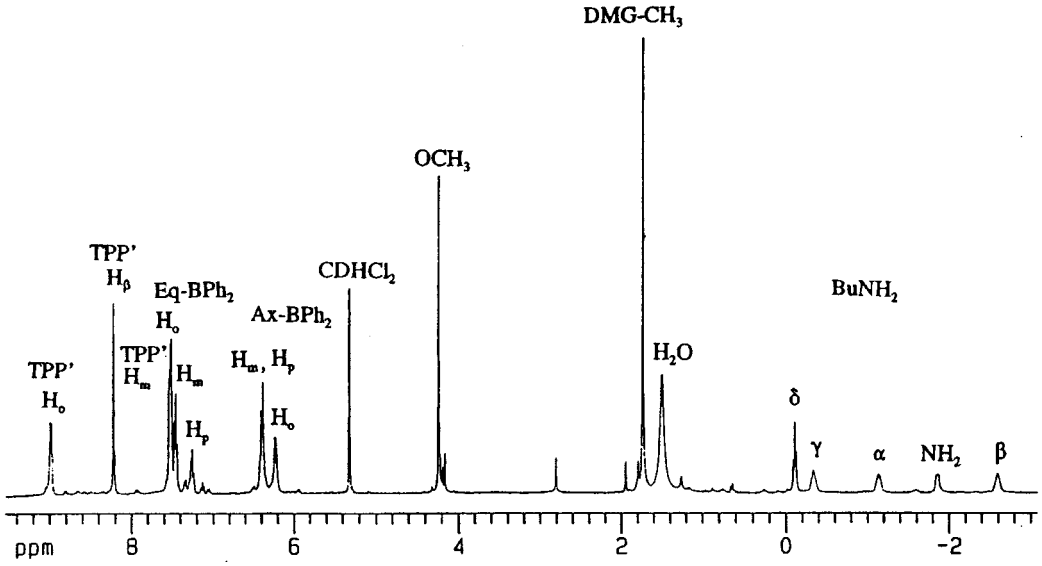

Figure 6. 400 MHz ^{1}H NMR spectrum of **2**-$(BuNH_2)_2$ in $CDCl_3$.

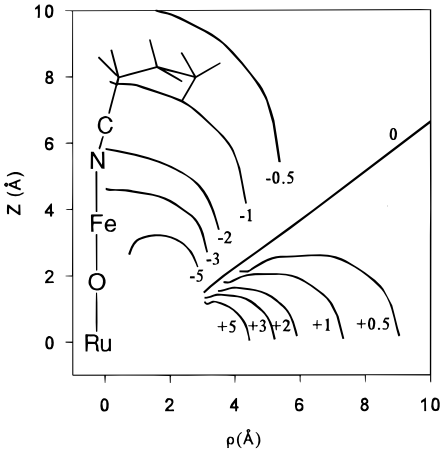

Figure 7. Porphryin ring current shifts based on the Abraham model.[18] *Z* and *ρ* are axial and equatorial coordinates; contours are in ppm. A part of a butyronitrile-ligated trinuclear species is shown.

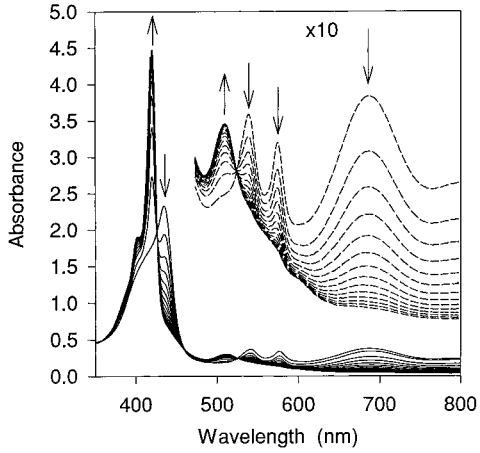

Figure 8. Visible spectral changes during reductive cleavage (eq 2) of **1**-$(CH_3CN)_2$ in CH_2Cl_2 at 25 °C. $[CH_3CN] = 0.40$ M, [4-*tert*-butylcatechol] = 0.002 91 M. Spectra were recorded at 10 min intervals.

$$[(CH_3CN)FeN_4{-}O]_2\,RuTPP' + 2H_2Q + 4CH_3CN \rightarrow RuTPP'(CH_3CN)_2 + 2FeN_4(CH_3CN)_2 + 2Q + 2H_2O \quad (2)$$

spectra.[10,19] The quinone product and overall stoichiometry were confirmed by NMR. No binuclear or other intermediates were detected. The isosbestic behavior requires that any binuclear intermediates be reduced more rapidly than the trinuclear species. A mechanism is outlined in Figure 9. The rate-determining step is proposed to involve H atom abstraction from a H-bonded precursor of reduced coordination number, leading directly to the quinone and $Fe^{II}{-}O{-}Ru^{IV}{-}O{-}Fe^{II}$. The $Fe^{II}{-}O{-}Ru^{IV}{-}O{-}Fe^{II}$ product then is proposed to break up rapidly into Fe^{II} and Ru^{IV} monomers. The oxo Ru^{IV} monomer would presumably be reduced rapidly by a second molecule of H_2Q before it would have time to dimerize to the more inert $Ru^{IV}{-}O{-}Ru^{IV}$ species.

The kinetics of reaction 2 were studied under pseudo-first-order conditions in CH_3CN and H_2Q, giving the rate law in eq 3. An inverse first-order dependence on $[CH_3CN]$ was also

$$-\mathrm{d}[Fe{-}O{-}Ru{-}O{-}Fe]/\mathrm{d}t = k_{obs}[Fe{-}O{-}Ru{-}O{-}Fe][H_2Q]/[CH_3CN] \quad (3)$$

observed in kinetic studies of H_2Q reduction of the analogous $Fe{-}O{-}Fe$ species.[7b] It seems that pentacoordination of the iron is a prerequisite to facile reduction of the μ-oxo bridge for both $Fe(III){-}O{-}Fe(III)$ and $Fe(III){-}O{-}Ru(IV)$ systems.

The rate constants for the trinuclear systems are summarized in Table 6 along with previous data for the binuclear systems.

(19) (a) Bonnet, J. J.; Eaton, S. S.; Eaton, G. R.; Holm, R. H.; Ibers, J. A. *J. Am. Chem. Soc.* **1973**, *95*, 2141. (b) Antipas, A.; Buchler, J. W.; Gouterman, M.; Smith, P. D. *J. Am. Chem. Soc.* **1978**, *100*, 3015. (c) Farrell, N.; Dolphin, D. H.; James, B. R. *J. Am. Chem. Soc.* **1978**, *100*, 324. (d) Collman, J. P.; Barnes, C. E.; Collins, T. J.; Brothers, P. J.; Gallucci, J.; Ibers, J. A. *J. Am. Chem. Soc.* **1981**, *103*, 7030. (e) Collman, J. P.; Barnes, C. E.; Swepston, P. N.; Ibers, J. A. *J. Am. Chem. Soc.* **1984**, *106*, 3500. (f) Barley, M.; Dolphin, D.; James, B. R.; Kirmaier, C.; Holten, D. *J. Am. Chem. Soc.* **1984**, *106*, 3937. (g) Tait, C. D.; Holten, D.; Barley, M. H.; Dolphin, D.; James, B. R. *J. Am. Chem. Soc.* **1985**, *107*, 1930. (h) Collman, J. P.; Brauman, J. I.; Fitzgerald, J. P.; Hampton, P. D.; Naruta, Y.; Sparapany, J. W.; Ibers, J. A. *J. Am. Chem. Soc.* **1988**, *110*, 3477. (i) Collman, J. P.; Brauman, J. I.; Fitzgerald, J. P.; Sparapany, J. W.; Ibers J. A. *J. Am. Chem. Soc.* **1988**, *110*, 3486. (j) Ke, M.; Sishta, C.; James, B. R.; Dolphin, D.; Sparapany, J. W.; Ibers, J. A. *Inorg. Chem.* **1991**, *30*, 4766. (k) Collman, J. P.; Garner, J. M.; Hembre, R. T.; Ha, Y. *J. Am. Chem. Soc.* **1992**, *114*, 1292. (l) Ohtake, H.; Higuchi, T.; Hirobe, M. *J. Am. Chem. Soc.* **1992**, *114*, 10660. (m) Pacheco, A.; James, B. R.; Rettig, S. J. *Inorg. Chem.* **1995**, *34*, 3477. (n) Pomposo, F.; Carruthers, D.; Stynes, D. V. *Inorg. Chem.* **1982**, *21*, 4245. (o) Funatsu, K.; Kimura, A.; Imamura, T.; Ichimura, A.; Sasaki, Y. *Inorg. Chem.* **1997**, *36*, 1625.

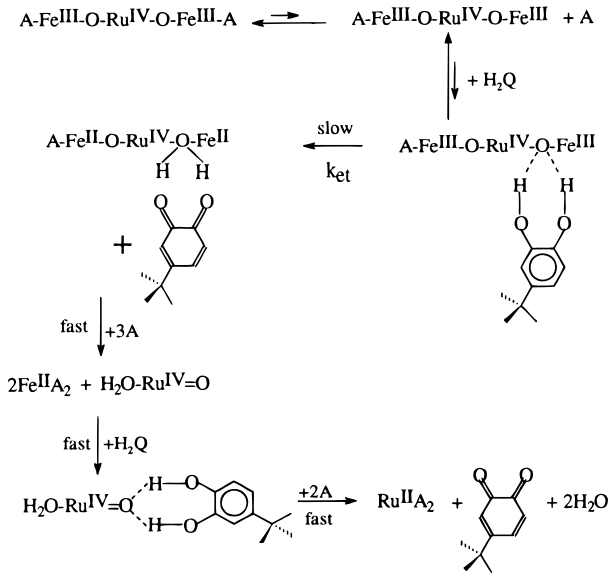

Figure 9. Reaction mechanism. A = CH_3CN.

Table 6. Kinetic Data for Reductive μ-Oxo Cleavage of Bi- and Trinuclear Complexes with 4-*tert*-Butylcatechol (H_2Q) in CH_2Cl_2 at 25 °C k (s^{-1})[a]

compd no.	N_4	$[LFeN_4O]_2RuTPP'$	$[LFeN_4]_2O$
1	$((DMG)BF_2)_2$	0.0453	220
2	$((DMG)BPh_2)_2$	slow	0.00436
3	$((DPG)BF_2)_2$	0.134	295[b]

[a] $k = k_{obs}[CH_3CN]/[H_2Q]$; estimated error 5%. [b] Segal, G. Unpublished results.

The reactivity order is **3** ≥ **1** ≫ **2** for both binuclear and trinuclear complexes. The trinuclear systems react 10^3-10^4 times more slowly than the binuclear iron analogues in all cases. The much slower reactivity of the trinuclear systems suggests that the Fe−O bond is stabilized by the Ru(IV). This could occur via greater π delocalization of oxo lone pairs onto ruthenium.

The trends in the rates for the three systems do not correlate with electronic effects or redox data but may be understood in terms of steric factors related to the bending of the oxo bridge in the pentacoordinate intermediate. Structural data for the $[Fe((DMG)BPh_2)_2]_2O$ system show that the bending of the Fe−O−Fe bond is facilitated when the Fe is pentacoordinate, as the Fe atom is displaced 0.3 Å out of the N_4 plane toward the oxo group and the peripheral structure is folded back over the vacant site.[7c] The smaller BF_2 groups in **1** and **3** permit a much greater bending back of the N_4 macrocycle and its superstructure than is possible with the BPh_2 groups in **2**. This would facilitate access to the oxo site and lower the barriers for the required rehybridization of the oxo oxygen atoms.[20] The basicity of the oxo lone pairs and the reduction of the iron are made more favorable in a bent pentacoordinate geometry. A lower coordination number will also generally favor the lower oxidation state.

These results provide insight into how the reactivity of the μ-oxo group may be controlled via peripheral structural effects of the metal coordination sphere. This can be a distinct advantage in controlling the rates of redox reactions, which usually are largely dependent on the thermodynamic driving force. The μ-oxo ligand produces both a thermodynamic and a kinetic stabilization of the higher oxidation levels of metal complexes. Cleavage of the μ-oxo bridge can provide a release of the oxidative power stored therein either by exposure of a much more reactive terminal oxo group or via the large redox potential changes which would accompany a change in the ligand sphere around one of the metals. While most discussions of the action of oxo-bridged metalloenzymes consider only the intact cluster,[2c,3d] it seems likely that systems which make use of oxo bridge cleavage as part of their activity will be found.

Summary. A variety of linear chain oxo-bridged heterotrinuclear systems can be obtained via reaction of terminal oxo complexes with low-spin FeN_4 complexes. The enhanced stability of systems involving the low-spin FeN_4 complexes, their strong oxidizing character, and the ability to append additional moieties via coordination to the terminal sites make these useful additions to the large number of multinuclear μ-oxo metal complexes now known.

Acknowledgment. We thank Robert Metcalfe and Mehrdad Ebadi for help with the electrochemical measurements. Financial support from the NSERC (Canada) is gratefully acknowledged.

Supporting Information Available: Tables of crystal data, atomic coordinates, thermal parameters, and bond distances and angles for **3**-$(BuNH_2)_2$, a table of kinetic data for reaction 2, and a visible spectrum of **2**-$(BuNH_2)_2$ (16 pages) Ordering information is given on any current masthead page.

IC9710162

(20) Caroll, J. M.; Norton, J. R. *J. Am. Chem. Soc*. **1992**, *114*, 8744.